

## Application of the harmonic balance method for ship-cargo interaction with intermittent contact nonlinearities

Speksnijder, A. D.; Karacadagli, U.; Seyffert, H. C.; Grammatikopoulos, A.

**DOI**

[10.1016/j.jsv.2024.118925](https://doi.org/10.1016/j.jsv.2024.118925)

**Publication date**

2025

**Document Version**

Final published version

**Published in**

Journal of Sound and Vibration

**Citation (APA)**

Speksnijder, A. D., Karacadagli, U., Seyffert, H. C., & Grammatikopoulos, A. (2025). Application of the harmonic balance method for ship-cargo interaction with intermittent contact nonlinearities. *Journal of Sound and Vibration*, 601, Article 118925. <https://doi.org/10.1016/j.jsv.2024.118925>

**Important note**

To cite this publication, please use the final published version (if applicable). Please check the document version above.

**Copyright**

Other than for strictly personal use, it is not permitted to download, forward or distribute the text or part of it, without the consent of the author(s) and/or copyright holder(s), unless the work is under an open content license such as Creative Commons.

**Takedown policy**

Please contact us and provide details if you believe this document breaches copyrights. We will remove access to the work immediately and investigate your claim.

Contents lists available at [ScienceDirect](https://www.sciencedirect.com)

## Journal of Sound and Vibration

journal homepage: [www.elsevier.com/locate/jsvi](http://www.elsevier.com/locate/jsvi)

# Application of the harmonic balance method for ship-cargo interaction with intermittent contact nonlinearities

A.D. Speksnijder<sup>a,b</sup>, U. Karacadagli<sup>b</sup>, H.C. Seyffert<sup>a</sup>, A. Grammatikopoulos<sup>a</sup>\*

<sup>a</sup> Department of Maritime & Transport Technology, Delft University of Technology, The Netherlands

<sup>b</sup> BigLift Shipping, The Netherlands

## ARTICLE INFO

### Keywords:

Harmonic balance method  
Hydrodynamic loading  
Intermittent contact  
Nonlinear bending vibrations  
Ship-cargo interaction

## ABSTRACT

An important trend exhibited by the offshore wind market is the increasing size of wind turbines, leading to longer and stiffer monopiles with larger diameter-to-thickness ratios. Current transport analysis is focused on loads resulting from hydrodynamic accelerations, without taking into account the loads resulting from differences in bending deflection between the vessel and cargo. This investigation examines the structural response of a monopile and sea-fastening system subjected to displacement-based loads. The load case follows from a vessel excited using a regular wave leading to bending deflections and rigid body accelerations. The intermittent contact between the saddles and monopile is modeled by representing the saddle with a unilateral spring. This requires the use of a nonlinear solution method to obtain structural responses. The harmonic nature of hydrodynamic-based loads led to the selection of the harmonic balance method (HBM) to model the cargo-sea-fastening system. A novel understanding is gained of how cargo properties, sea-fastening properties, and sea-fastening arrangements influence the structural response of the coupled cargo-sea-fastening system. Various parametric studies are performed to identify behaviors related to the total structural response. Based on this study, the conclusion can be drawn that a large number of saddles in combination with a low stiffness is desired to minimize the structural response of the cargo and sea-fastening system. Furthermore, the influence of lashing stiffness and pretension is limited with respect to the total response. Both these conclusions also hold for an increase in cargo length and diameter.

## 1. Introduction

Within the offshore wind market, there is a significant trend towards larger wind turbines in terms of power and size, with expected rotor diameters exceeding 250 meters by 2030 [1,2]. As a result, the monopiles used as foundations will also increase in size [3]. Concerns arise that this increase in size could affect the transport operation. Current transport analysis is focused on loads induced by rigid-body motions, without taking into account the influence of differences in bending deflection between the vessel and cargo on the load distribution.

Conventional sea-fastening systems applied for monopile transportation consist of several components. Firstly, a set of saddles supports the monopile's weight and spreads the forces across the vessel (an example can be seen in Fig. 1). These saddles function as unilateral constraints, only exerting a reaction force when compressed. When the saddle is loaded in tension past its equilibrium, separation and, consequently, intermittent contact occurs. Friction is also introduced through the contact between the saddles and

\* Corresponding author.

E-mail address: [A.Grammatikopoulos@tudelft.nl](mailto:A.Grammatikopoulos@tudelft.nl) (A. Grammatikopoulos).

<https://doi.org/10.1016/j.jsv.2024.118925>

Received 26 September 2024; Received in revised form 16 December 2024; Accepted 23 December 2024

Available online 30 December 2024

0022-460X/© 2024 The Authors.

Published by Elsevier Ltd.

This is an open access article under the CC BY license

(<http://creativecommons.org/licenses/by/4.0/>).

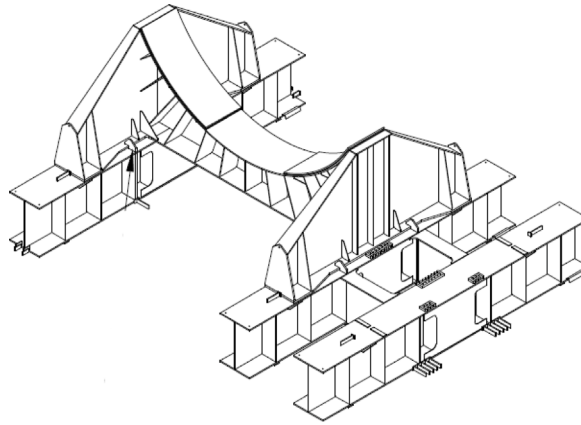


Fig. 1. Monopiles are typically loaded on top of several saddles, which are welded on the main deck of the vessel.

the monopile, when the latter moves in the axial direction. Stability in the axial direction is reinforced by the use of lashing wires, which provide a restoring force. The lashing wires are installed under an angle, so they can generate a vertical restoring force as well. The wires can be modeled using linear theory, because they are pretensioned and therefore are always in tension. The friction force, on the other hand, introduces further nonlinearities due to its dependency on normal force and relative velocity. As a result, it is expected that, for some combinations of system parameters and loading regimes, the structural response cannot be described by linear vibration theory, emphasizing the need for a nonlinear analysis method.

Research related to ship-cargo interaction focuses on shifting of granular cargo and resulting instabilities [4,5], sloshing and its influence on dynamics [6–8] and multi-body dynamics related to lifting operations [9–13]. This research cannot provide any insight regarding the problem at hand, as the monopiles are a continuous type of cargo of comparable size and stiffness to the ship, emphasizing the importance of the interacting flexible responses of both structures. Research concerning the impact of stiff cargo on dynamic behavior and structural response is limited. A specific study has shown the influence of the on the mode shapes, load distribution and eigenfrequencies [14], but some limitations were identified: hydrodynamic contributions were excluded and linear modeling was applied. This emphasizes the need for further research.

Given the absence of related literature, the problem is simplified and modeled in 2D, namely in the symmetry plane of the vessel. Additionally, axial responses for neither structure are considered and, therefore, nonlinearities due to frictional constraints are not included. This enables investigating the influence of the nonlinearity solely due to intermittent contact, instead of introducing additional nonlinearities.

Intermittent contact problems have been analyzed in a nonlinear manner in various disciplines. In the aerospace industry, multiple studies investigate the contact problem between blade-tip and casing for gas turbines [15,16]. In both examples, the nonlinear problem is solved in frequency domain using the harmonic balance method. A different solution approach involves creating a piecewise linear system, with transition times where contact or loss of contact occurs [17,18]. Finally, in the field of soil mechanics the intermittent contact problem is also relevant, with a solution presented in [19]. In this investigation, the authors make use of the shooting method to solve the problem, which operates in the time domain.

In this study, the structural response of a monopile and sea-fastening system subjected to displacement-based loads is investigated. The load case follows from a vessel excited using a regular wave leading to bending deflections and rigid body accelerations. The objective of this study is to create an efficient model capable of defining the structural response of the cargo and sea-fastening system, taking the intermittent contact nonlinearities between the ship and cargo by into account. The harmonic balance method is selected due to the harmonic nature of hydrodynamic loads, in combination with the numerical efficiency of the method. Using this model, various parametric analyses are performed to evaluate the importance of nonlinear behavior.

In Section 2 the base case, including parameters related to the vessel and the cargo and a general outline of the model, is described. Section 3 introduces the hydrodynamic part of the model, and how it serves as excitation. The mathematical background to model the structural side of the problem is presented in Section 4. Section 5 follows up on this by presenting the results for an in-depth analysis of the dynamic response under hydrodynamic loading. The parameters of the dynamics system are varied in a systematic way and their impact on nonlinear dynamic behavior is assessed in Section 6.

## 2. Problem definition

In this investigation, an MC-class heavy-lift vessel is considered, as these vessels are used to carry the largest monopiles, as shown in Fig. 2.

The main particulars of the vessel and the cargo are shown in Table 1.  $L$  represents length,  $B$  breadth,  $D$  diameter,  $T$  draft,  $V$  displacement (or mass of the vessel),  $t$  the thickness, and  $I$  the second moments of area of the vessel's midship section and of the cross section of the monopile, respectively. It is evident that the length of the cargo is significant compared to the length of the



Fig. 2. Base case MC-class heavy-lift vessel transporting monopiles.

Table 1

Main particulars MC-class heavy-lift vessel and monopile cargo.

Parameter	Value	Parameter	Value
$L_s$ [m]	171	$L_m$ [m]	74
$B_s$ [m]	42	$D_m$ [m]	8
$T_s$ [m]	6.5	$t_m$ [mm]	8
$\nabla_s$ [m <sup>3</sup> ]	32000	$I_m$ [m <sup>4</sup> ]	15.6
$I_s$ [m <sup>4</sup> ]	103.8		

(a) Ship particulars

(b) Cargo particulars

vessel, in this case approximately 43%, which means that it can no longer be considered a point mass. Furthermore, since both the vessel and monopile are manufactured using steel, when the vessel is carrying four monopiles the bending stiffness of the cargo also becomes comparable to that of the vessel.

Fig. 3 depicts a schematic representation of Fig. 2, illustrating the model's components in part (A). Part (B) depicts the transfer of loading from the linear hydrodynamic model to the nonlinear structural model. Excitation is present within the structural model at the locations of the components of the sea-fastening system. The hydrodynamic model generates a bending response of the vessel which is quasi-statically transferred to the cargo by transforming the accelerations and bending deflections into a displacement-based load, i.e., a base excitation, at the saddle points. These loads are represented by the red and green arrows, respectively.

For simplification purposes, only one-way coupling between the ship and the cargo is applied, meaning that the deflections of the ship are unaffected by the deflections of the cargo. It is expected that the stiffness contributions of the cargo will be affecting the natural frequencies of the coupled system, as demonstrated previously with linear analysis [14]. However, this study also showed that whether the vibrations of ship and cargo are considered separately or as a combined system, the resulting natural frequencies are at least an order of magnitude above the wave excitation frequency. Consequently, and as will be confirmed later in the present investigation, the deflections of the monopile are expected to be sufficiently small that their influence on the deflections of the hull can be considered insignificant.

Finally, in part (B) of Fig. 3, the discretization of the cargo into elements with  $z$  and  $\theta$  as degrees of freedom is depicted. Mesh density was selected so that all interaction with the sea-fastening system, such as a lashing or saddle loads, could be applied at nodal locations (after convergence). A global system of equations, including the contributions of the sea-fastening system, was derived. The resulting models are discussed in the following sections, along with their mathematical representation.

### 3. Hydrodynamic model

This model defines the accelerations and bending deflections of the vessel, based on quasi-statically applied hydrodynamic loads, which are in turn calculated using a potential flow code. Both the hydrodynamic and structural models for the vessel are linear. The deflections are first calculated for the entire vessel and then evaluated at the locations of the saddles.

#### 3.1. Deflection-induced loads

The deflections of the vessel for each combination of wave length and wave amplitude are determined using a quasi-static approach. A force equilibrium between the gravitational and buoyant forces is used to produce the bending moment applied to the vessel. Using the stiffness distribution of the vessel, the resulting deflections can be calculated. The deflection of the vessel consists of 2 parts: the hydrostatic and wave-induced deflection, as shown in Fig. 4. In this figure, the wave-induced component is calculated

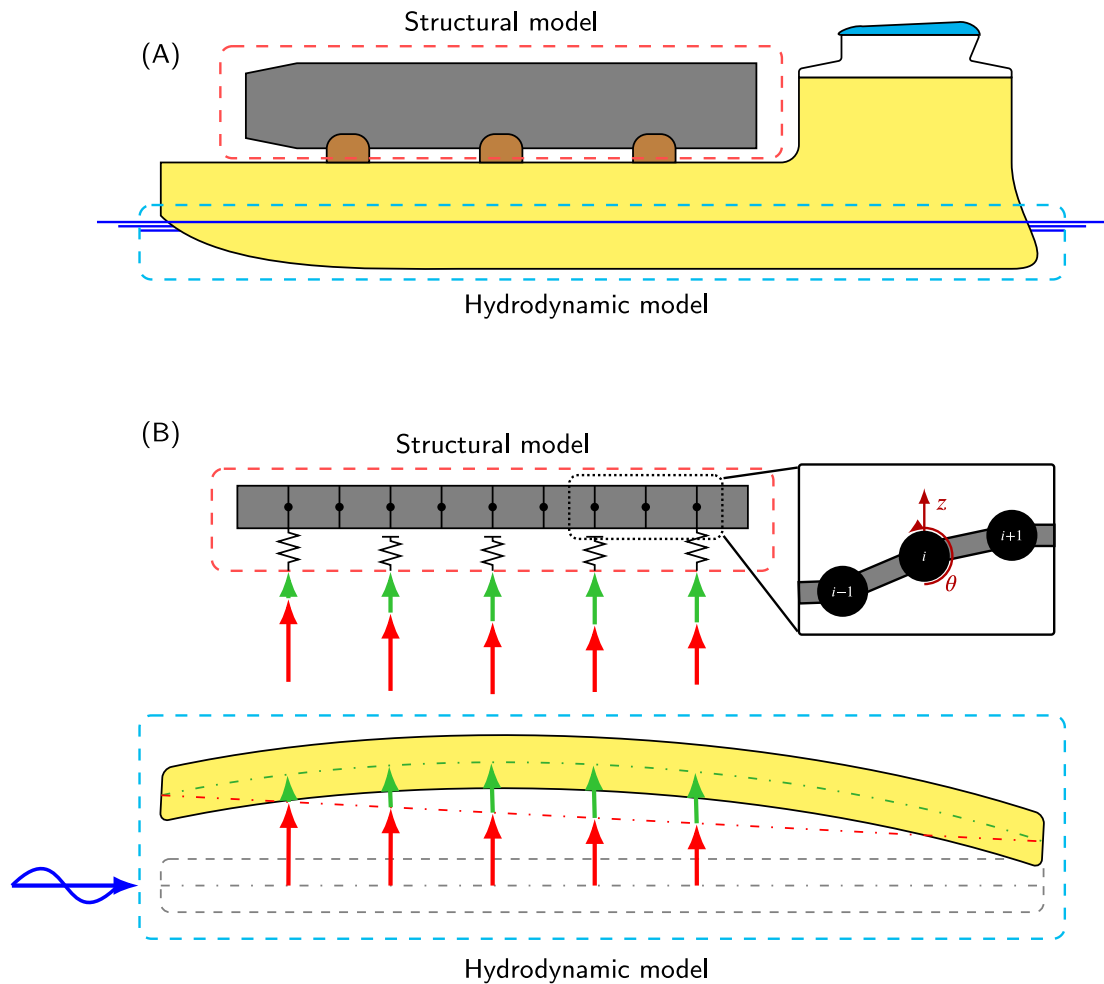


Fig. 3. Schematics of the sub-models required and their interactions. (A) Illustrates these divisions in the real-world problem and (B) demonstrates the characteristics of each mathematical model and the points of interaction.

for a wave length of 171 m, equal to the vessel length, and a wave amplitude of 1 meter. This corresponds to a wave frequency of 0.6 rad/s, assuming deep water. The first natural frequency of the system, assuming linear behavior, is approximately 25 rad/s, hence more an order of magnitude higher than the expected excitation frequencies. Since the natural frequencies of the structure are too high for resonance to occur due to wave excitation, the situation when the wave length matches the ship length is expected to generate the maximum bending moment. Simulations in a range of different frequencies around this region provided no evidence of sub-harmonic response, confirming that ship-wave matching is the worst possible scenario.

### 3.2. Inertial loads

The rigid-body accelerations of the vessel cause inertial loads on the cargo and sea-fastening system. These rigid body accelerations are calculated through a diffraction analysis for various wave loads and frequencies on the vessel. Fig. 5 shows the response amplitude operators for the heave and pitch motions of the vessel.

## 4. Structural model

This section defines the mathematical representation of the cargo and sea-fastening in a structural model, as shown in Fig. 3. A linear and a nonlinear version of the model were generated to clearly identify the importance of nonlinear contributions. The two models were otherwise very similar to each other, as will become evident from their detailed descriptions below.

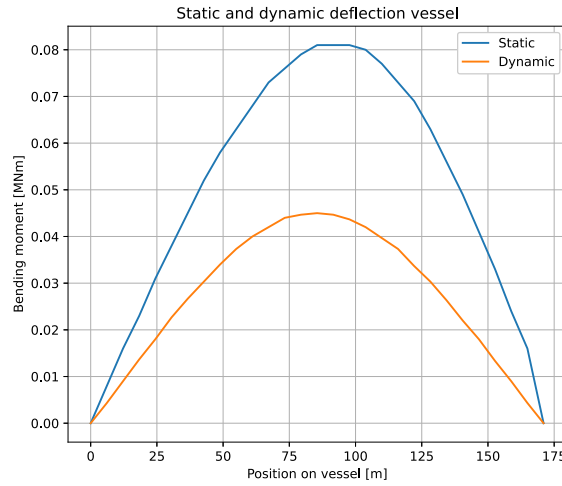


Fig. 4. Comparison of static (hydrostatic) and dynamic (wave-induced) deflection of vessel.

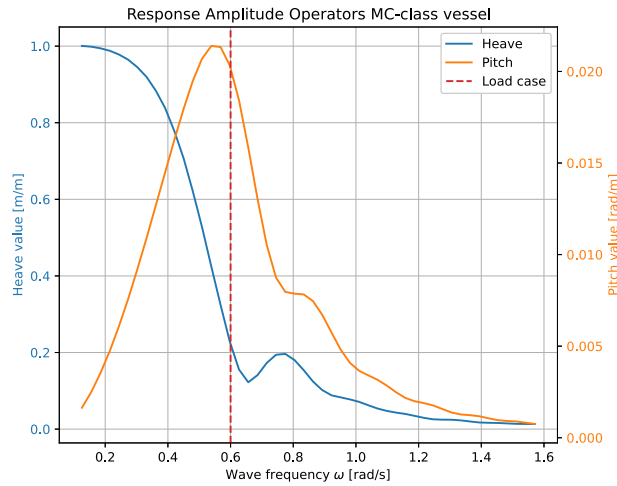


Fig. 5. Rigid-body motion response amplitude operators for MC-class heavy-lift vessel. Here the frequency of the considered load case, corresponding to a wave length equal to the ship length, is shown by the red dashed line. (For interpretation of the references to color in this figure legend, the reader is referred to the web version of this article.)

#### 4.1. Linear structural model

The cargo is discretized using a Timoshenko beam finite element formulation, due to the limited slenderness of these types of vessels. Euler–Bernoulli beam theory was used for the monopiles, as their length is far greater than their diameter.

The generalized equation of motion used within the FEA framework [20] is included below (Eq. (1)). Parameters  $\mathbf{M}$ ,  $\mathbf{D}$  and  $\mathbf{K}$  represent the global mass, damping, and stiffness matrices, respectively. Parameter  $\mathbf{x}$  is a vector representing all the degrees of freedom in the system, equal to twice the number of nodes, for degrees of freedom  $z$  and  $\theta$ . Finally, parameter  $\mathbf{f}_{ex}$  is the vector representation of a general excitation force.

$$[\mathbf{M}]\ddot{\mathbf{x}} + [\mathbf{D}]\dot{\mathbf{x}} + [\mathbf{K}]\mathbf{x} = \mathbf{f}_{ex} \quad (1)$$

Because of the harmonic nature of wave loads, the response  $\mathbf{x}$  can also be assumed to be harmonic. The equation can therefore be translated into the frequency domain, as shown in Eq. (2), where  $\omega$  represents the excitation frequency. Finally, the external harmonic forcing  $\mathbf{f}_{ex}$  will have nonzero values at the locations where the displacement is enforced.

$$\begin{aligned} x_i &= x_{i,a} \cdot \sin(\omega t) \\ (-\omega^2[\mathbf{M}] + \omega[\mathbf{D}] + [\mathbf{K}]) \mathbf{x} &= \mathbf{f}_{ex} \end{aligned} \quad (2)$$

Responses to forced displacement load cases can be evaluated using matrix partitioning. The equation of motion is split into 2 parts, based on known and unknown displacements. Matrix partitioning is required, as the monopile is subjected not only to a

displacement/base excitation, but also forced bending. Therefore, conventional base excitation formulations, where everything is calculated as relative displacements, would not be sufficient. Eq. (3) shows the first step in the partition; for simplicity, the matrices used in Eq. (2) are summarized into a dynamic stiffness matrix  $K_d$ .

$$\mathbf{K}_d = (-\omega^2[\mathbf{M}] + \omega[\mathbf{D}] + [\mathbf{K}]) \quad (3)$$

$$[\mathbf{K}_d] \mathbf{x} = \mathbf{f}_{ex}$$

From there, the equation can be split further for a known displacement vector  $\mathbf{x}^o$  and an unknown displacement vector  $\mathbf{x}^c$ . The dynamic stiffness matrix  $K_d$  must be split accordingly, resulting in 4 submatrices as shown in Eq. (4). Finally, external harmonic force vector  $\mathbf{f}_{ex}$  is also split into 2 vectors corresponding to known and unknown displacement degrees of freedom. In order to solve this equation, either the applied force must be known for a degree of freedom, denoted by  $\mathbf{f}_{ex}^c$ , or the displacement, denoted by  $\mathbf{x}^o$ . In the current situation the displacement vector  $\mathbf{x}^o$  consists of the displacements and rotations at the locations where the saddles are connected to the ship.

$$\begin{bmatrix} \mathbf{f}_{ex}^c \\ \mathbf{f}_{ex}^o \end{bmatrix} = \begin{bmatrix} \mathbf{K}_d^{cc} & \mathbf{K}_d^{co} \\ \mathbf{K}_d^{oc} & \mathbf{K}_d^{oo} \end{bmatrix} \begin{bmatrix} \mathbf{x}^c \\ \mathbf{x}^o \end{bmatrix} \quad (4)$$

Eq. (5) is produced by rewriting Eq. (4) and solving for the unknown displacement vector  $\mathbf{x}^c$  based on the known displacement vector  $\mathbf{x}^o$  and known force vector  $\mathbf{f}^c$ . The second part of the equation shows how the unknown forces  $\mathbf{f}^o$  are obtained, required to force the displacement.

$$\begin{aligned} \mathbf{x}^c &= [\mathbf{K}_d^{cc}]^{-1} [\mathbf{f}_{ex}^c - \mathbf{K}_d^{co} \mathbf{x}^o] \\ \mathbf{f}_{ex}^o &= \mathbf{K}_d^{oc} \mathbf{x}^c - \mathbf{K}_d^{oo} \mathbf{x}^o \end{aligned} \quad (5)$$

The accelerations and bending deflections resulting from the hydrodynamic model can be transformed into a single displacement. Appendix A shows a comparison between the loads resulting from forced bending deflections and accelerations, for a simple cargo and sea-fastening system. For this example a wave amplitude of 1 meter was used. This example shows that the forces caused by forced bending far exceed the inertial forces caused by accelerations.

The static deflections of the monopile and sea-fastening, resulting from gravitational forces and hydrostatic deflections of the vessel, are also obtained using Eq. (4) and (5). The hydrostatic deflections of the vessel are included in displacement vector  $\mathbf{x}^o$ , while the weight of the monopile is distributed over the nodes and included in  $\mathbf{f}_{ex}^c$ . Note that in this situation the dynamic stiffness matrix  $\mathbf{K}_d$  is equal to the structural stiffness matrix  $\mathbf{K}$ . The resulting deflections can be superimposed on the dynamic deflections to obtain the total response.

#### 4.2. Nonlinear solver

A nonlinear solution method is required to handle the nonlinearities introduced by the saddles. Eq. (6) contains the general formulation for structural vibration in the presence of nonlinear forces [21]. The solution here is represented by  $\mathbf{q}$  instead of  $\mathbf{x}$ , to highlight the difference between the linear and nonlinear solution. The nonlinear force term  $\mathbf{f}_{nl}(\mathbf{q}, \dot{\mathbf{q}})$  defines the total nonlinear force for elements within the system dependent on the displacement  $\mathbf{q}$  or velocity  $\dot{\mathbf{q}}$ .

$$\begin{aligned} [\mathbf{M}]\ddot{\mathbf{q}} + [\mathbf{D}]\dot{\mathbf{q}} + [\mathbf{K}]\mathbf{q} + \mathbf{f}_{nl}(\mathbf{q}, \dot{\mathbf{q}}) &= \mathbf{f}_{ex}(t) \\ \mathbf{f}_{ex}(t) &= \mathbf{f}_{ex}(t + T) \end{aligned} \quad (6)$$

The equation of motion can be solved numerically using various solution techniques, for example the shooting method [22], harmonic balance [21] method and intermediate methods [23]. The assumption is made that the nonlinear forces and responses can be represented as a summation of harmonics, as stated by the harmonic balance method. This approach has been demonstrated to be compatible with problems involving harmonic excitation and unilateral constraints [18].

In Eq. (7), the equation of motion is rewritten in the frequency domain, with the solution expressed as a truncated Fourier series. Note that the periodic character of the excitation force has been removed. Rewriting the equation in this form results in a system of  $n \cdot (2H + 1)$  equations. Parameter  $n$  represents the number of degrees of freedom present in the discretized system, for which a zero frequency term, a sine, and a cosine term are present. The sine and cosine terms are present for every harmonic, up to harmonic  $H$ . Parameter  $k$  represents the harmonic considered in each term of the summation.

$$\begin{aligned} \mathbf{q}(t) &= \mathbf{Q}_0 + \sum_{k=1}^H \mathbf{Q}_{c,k} \cos k\omega t + \sum_{k=1}^H \mathbf{Q}_{s,k} \sin k\omega t \\ &= \Re \left\{ \sum_{k=0}^H \mathbf{Q}_k e^{ik\omega t} \right\} \\ \Re \left\{ \sum_{k=0}^H \left( [-k\omega]^2 [\mathbf{M}] + ik\omega [\mathbf{D}] + [\mathbf{K}] \right) \mathbf{Q}_k + \mathbf{f}_{nl,k} \right\} &= \mathbf{f}_{ex,k} \end{aligned} \quad (7)$$

For the purposes of this work, the Harmonic Balance algorithm provided in the NLvib (v1.3) package, developed at the University of Stuttgart [21], after being translated from MATLAB to Python.

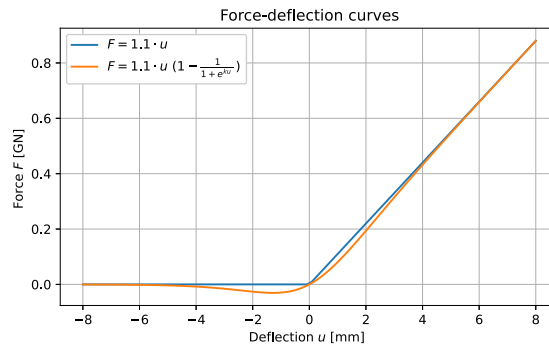


Fig. 6. Force–deflection curves for different saddle stiffness formulations.

#### 4.2.1. Description of nonlinear force

Here, the nonlinear force vector  $\mathbf{f}_{nl,k}$  described in Eq. (7) is analyzed in more depth. The force–deflection curve for a unilateral linear spring is shown in Fig. 6. The desired curve is shown in blue and the regularized curve in green. For the saddles considered in this investigation, a stiffness  $k_{sad}$  of  $1.1 \cdot 10^{11}$  N/m in compression was identified. However, the function shown in Eq. (7) is solved using an AFT solver which requires a force–displacement curve with  $C^0$  and  $C^1$  continuity. If the above is not satisfied, significant convergence issues are encountered. Therefore, it is necessary to apply force regularization on the original force–deflection curve, which is not  $C^1$  continuous at 0. The regularized curve, shown in green fulfills the smoothness requirements for the entire range of deflections. Note that  $k$  in this function is the regularization parameter. This value has been set to 1000 to have sufficient accuracy around a deflection of the saddle of 5 millimeters. The importance of this level of accuracy will be further discussed in a later section.

The quality of the solution highly depends on the extent to which the nonlinear force can be described using harmonics [21]. Three potential solution strategies are identified to define the nonlinear force harmonics  $\mathbf{f}_{nl,k}$  [21]:

1. For polynomial nonlinear forces: solve for closed-form expression
2. For piecewise polynomial forces: determine transition times, proceed as in 1
3. For generalized (i.e. non-polynomial) nonlinear forces: apply Alternating Frequency–Time (AFT) scheme

Within this problem, the usage of Alternating Frequency–Time is selected to define the nonlinear force harmonics. Due to the number of unilateral constraints present in the problem, it is hard to define the transition times between different states. Fig. 7 shows an example of the AFT procedure applied for this case. The blue curve represents the deflection of the saddle, and a negative deflection indicates separation of the saddle and the monopile, which should result in a zero contact force. The green curve represents the nonlinear force in the time domain, which is based on the aforementioned deflection of the saddle. This force is obtained using the regularized force–deflection description shown in Fig. 6. This green curve is then approximated using 5 harmonics (and 128 time steps in the time domain), the sum of which is represented by the red curve. A slight tensile force on the saddle is observed on both the green curve and the red curve; this error is a by-product of the regularization of the force curve. Finally, an appropriate number of harmonics needs to be chosen to converge to the time domain force, to represent it accurately.

#### 4.2.2. Continuation method

In conventional nonlinear vibration analysis the solution method is applied together with a continuation method. Examples of continuation methods include the Asymptotic Numerical Method (ANM) [24] and pseudo-arclength continuation [22]. Such methods allow to identify and map bifurcations in the dynamic behavior of the system. For this investigation, and based on pinned boundary conditions at both ends of the monopile (which is a reasonable assumption for the linear problem), an eigenfrequency of 25 rad/s is identified. Since the excitation only has a frequency of 0.6 rad/s, it was concluded that this load case is located away from resonance, and consequently characterized by low energy. Additionally, the nonlinearity, although expressed in the form of a nonlinear stiffness, is not expected to create bifurcating behavior; the main stiffness sources of stiffness are the monopile and the sea-fastening system, and the nonlinearity relates primarily to a re-distribution of the bending loads and the elimination of an over-constrained system. Therefore, behavior related to bifurcations, bending, and jumping is not expected. Consequently, no continuation methods were applied, and the investigation focused on the comparison between linear and nonlinear predictions for the problem at hand.

#### 4.2.3. Residual function & solver

The numerical solver requires the equation of motion to be rewritten in residual form. Some reformulation is required to be able to apply a displacement-based excitation, resulting from the acceleration and bending of the vessel. The formulation is shown in Eq. (8). Matrix partitioning is applied again in combination with the definition of the dynamic stiffness matrix  $\mathbf{K}_d$ . The function

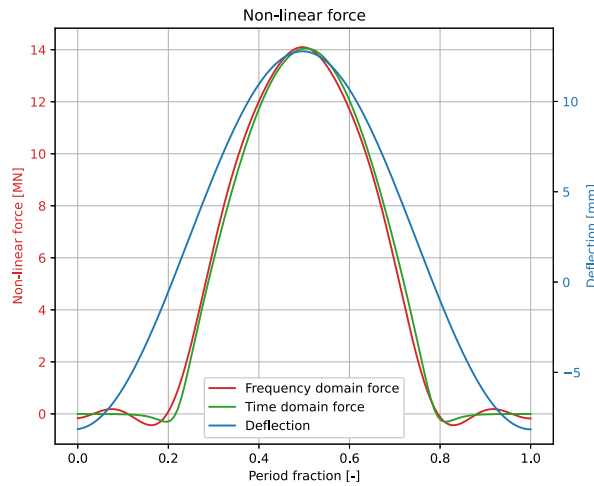


Fig. 7. Comparison of the nonlinear saddle stiffness force calculated in the time domain and frequency domain, using the Alternating Frequency–Time procedure.

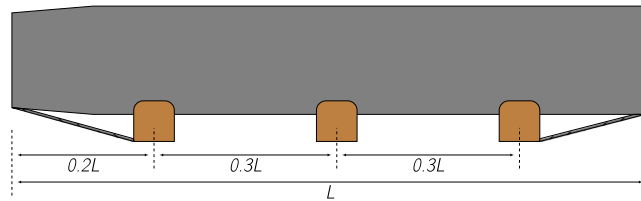


Fig. 8. Schematic overview sea-fastening system applied at monopiles in base case.

is rewritten in residual form, and this function represents the residual of a single harmonic  $k$ . The exciting force  $\mathbf{f}_{\text{ex},k}$  only has a value for  $k = 0$ , here the gravitational forces are distributed over the length of the monopile.

$$\begin{aligned} \mathbf{K}_d &= [-(k\omega)^2[\mathbf{M}] + (ik\omega)[\mathbf{D}] + [\mathbf{K}]] \\ \mathbf{R}_k &= [\mathbf{K}_d^{cc}] \mathbf{Q}_k^c + [\mathbf{K}_d^{oc}] \mathbf{x}^o + \mathbf{f}_{\text{nl},k} - \mathbf{f}_{\text{ex},k} = \mathbf{0} \end{aligned} \quad (8)$$

This residual function is then used in combination with the function Jacobian, within the Powell hybrid method. The Jacobian was defined using analytical derivatives, which ensures efficient solving of the function.

This concludes the modeling sections present within this problem. A modeling method was developed to transform a hydrodynamic load into displacements at the locations of the saddles. Subsequently, a structural model was introduced to evaluate the responses of the monopile and sea-fastening system using a displacement-based load. The following sections discuss application of this methodology to specific load cases.

## 5. Application: structural response for base case based on static and dynamic load

This section discusses the results for the base case as introduced in Section 2. Within this project the sea-fastening system was defined as shown in Fig. 8.

The various sea-fastening components needed to be translated into appropriate mathematical formulations to be included in the structural model. Fig. 9 shows the aft ends of the monopiles, where both a saddle and a lashing wire are applied. As depicted in the figure, both the saddle and lashing wire act in a unilateral manner and only provide reaction forces in compression and tension, respectively. A combination of both can therefore be modeled in a linear manner with spring stiffness  $k_z$ .

Since the stiffness of the saddle is far greater than the lashing wire, a unilateral spring with the remaining stiffness  $k_s$  is added. The lashing wire also provides some rotational resistance around the saddle, which is modeled as a linear rotational spring with stiffness  $k_\theta$ . The assumption is that the lashing wire will always be in tension by applying pre-tension, allowing the rotational spring to be modeled in a linear manner. Note that for the saddle located at  $0.5L$  only a unilateral spring with the total saddle stiffness is applied. Furthermore, the three spring elements shown in Fig. 9 are in the model all applied at the same location, being the location of the saddle. Finally, it is important to note that within the linear model the unilateral spring stiffness  $k_s$  is linearized, and added to the linear stiffness  $k_z$ .

Table 2 shows the parameters related to the sea-fastening system. Note that parameters  $k_z$  and  $k_\theta$  are based on the lashing stiffness  $k_l$ . It is common industry practice that a pre-tension of 1–2 mT is applied per lashing wire. This comes down to 10 kN per wire, so for the example case the total pre-tension  $T_l$  would be 210 kN.

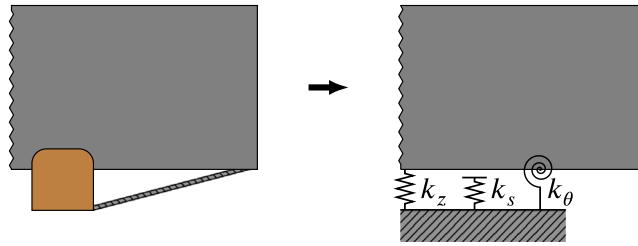


Fig. 9. Detailed version of monopile aft end with implementation of spring stiffnesses.

Table 2  
Structural parameters sea-fastening system.

Parameter	Value	Unit
$k_s$	1.1	GN/m
$k_f$	37.5	kN/m
$T_f$	210	kN
$k_z$	6.5	kN/m
$k_\theta$	1.46	MNm/rad

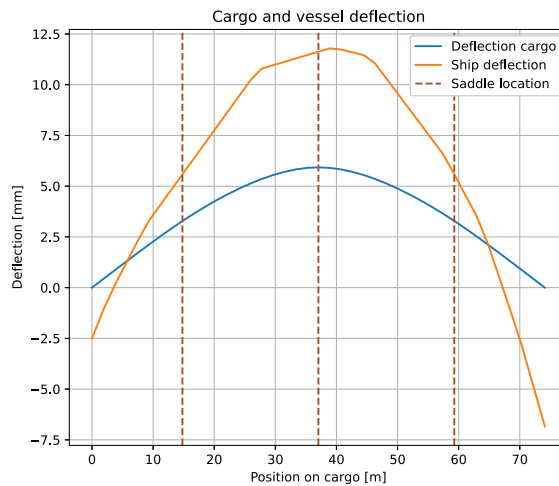


Fig. 10. Deflection of ship, saddles and monopile for hydrostatic (still water) load case.

Table 3  
Results for hydrostatic (still water) load case.

Parameter		Linear	Unit
Deflection mon. max.	$u_c$	5.9	mm
Deflection sad. max.	$u_d$	5.7	mm
Force max.	$F$	6.3	MN
Bending mom. max.	$M_b$	49.3	MNm

### 5.1. Static analysis

A static analysis is performed for the case presented in Section 2. In this situation, the cargo is subjected only to the hydrostatic deflection of the vessel and the gravitational forces acting on the monopile. The resulting deflections are shown in Fig. 10 and summarized in Table 3. In this figure the deflection of the saddle is defined by the difference between the cargo deflection and ship deflection curve. It was found that the deflection of the saddle located at  $0.5L$  is significant compared to the deflection of the monopile, and almost equal to the maximum deflection of the monopile.

Furthermore, Fig. 11 shows the distribution of forces and bending moments. Note that the force is slightly negative, caused by the distributed gravitational force. The unequal distribution of the weight of the monopile over the saddles is caused by the bending of the vessel. This bending increases the normal force in the middle saddle, and decreases the normal force in the outer two saddles. The high stiffness of the monopile causes the influence of the bending of the vessel on the weight distribution to become pronounced,

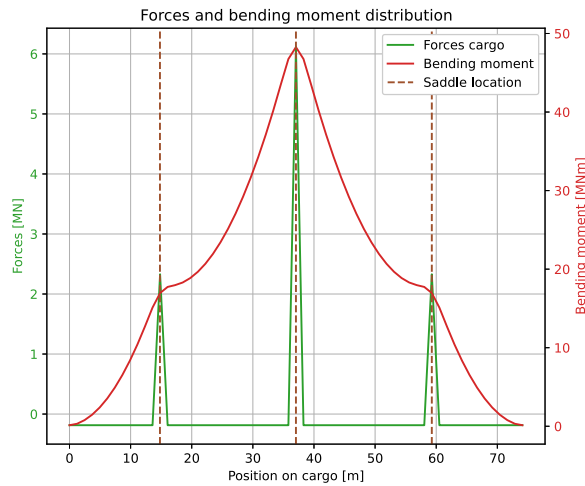


Fig. 11. Forces and bending moments acting on monopile.

**Table 4**  
Results dynamic load case using different models.

Parameter		Linear	Non-Lin.	Unit
Deflection mon. max.	$u_c$	13.4	11.4	mm
Deflection sad. max.	$u_s$	11.5	9.9	mm
Detachment max.	$u_d$	–	8.5	mm
Force max.	$F$	12.4	10.6	MN
Bending mom. max.	$M_b$	115.3	97.3	MNm
Bending stress max.	$\sigma_b$	29.6	25.0	MPa

since the bending deflections of the monopile under its weight stay limited. Therefore, a slight lift in the middle of the monopile results in the monopile being raised at the outer saddles. This then increases the normal force observed in the middle, but decreases the normal forces observed at the outer ends.

Appendix B shows the sensitivity of the observed force distribution under influence of the deflection of the saddles. A wrong saddle stiffness leads to wrong deflections into the saddles, which then affects the force and bending moment distribution. The example highlights the sensitivity of the system with respect to the forced deflection of the ship, the axial deflection of the saddles, and the resulting bending deflection of the monopile.

### 5.2. Dynamic analysis

The hydrodynamic load case used in the dynamic analysis has the following parameters. As mentioned earlier, the wave length  $L_w$  is assumed to be 171 m, corresponding to a wave frequency  $\omega$  of 0.6 rad/s. Furthermore, a wave amplitude  $\zeta_a$  of 3 meters is assumed. In this situation a high wave amplitude is chosen to amplify dynamic effects.

Fig. 12 shows the dynamic results for the force and deflection distribution for the nonlinear model. Note that in addition to the position on the cargo, the time step within the oscillation is also plotted on the period fraction axis.

That nonlinear behavior indeed occurs here is confirmed by both the nonlinear forces and deflections figures, shown in Figs. 12(a) and 12(b). These figures show that the normal force drops to 0 for the saddle located at  $0.8L$  and that detachment indeed occurs here, with a magnitude up to 8.5 millimeters. When the linear forces are evaluated using the linear model, a negative normal force is indeed observed at  $t = 0$ , for the outer saddles located at  $0.2L$  and  $0.8L$ .

Further results are summarized in Table 4. This table shows that the deflection, forces, and bending moments are overestimated by a linear approach. This is caused by the problem being overconstrained when linearizing a nonlinear constraint. Table 4 also shows that the bending stress in the monopiles stays limited compared to the yield stress.

Finally, the peak observed at a period fraction of 0.1 for the normal force of the saddle located  $0.5L$  is caused by the slight tensile force present at the saddle of  $0.8L$ . A similar situation as shown in Fig. 7 occurs here: the small negative deflection leads to a small tensile force. This behavior results in the maximum force being overestimated. If the magnitude of this peak is compared to the overall force, the conclusion can be drawn that the magnitude of this error stays limited.

### 5.3. Discussion

Based on the static and dynamic analysis some observations can be made:

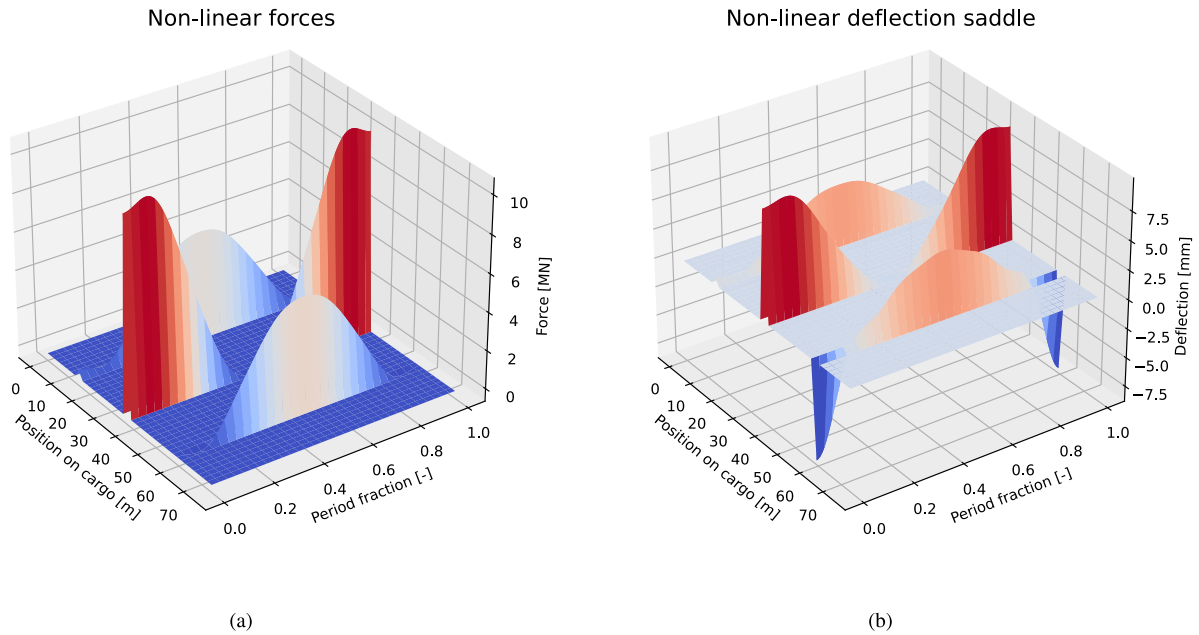


Fig. 12. Forces and deflections in sea-fastening system for nonlinear analysis. The locations in the nonlinear force plot, shown in the left figure, indicate time instances where detachment occurs. This is confirmed by the right figure, indicating the magnitude of detachment.

- The static analysis shows that the force distribution is dependent on the bending deflection of the vessel, the axial deflection of the saddles, and the bending deflection of the monopile under its weight.
- Slight changes in saddle deflection can lead to a large difference in force distribution.
- The observed deflections of saddles and the monopile are in the same order of magnitude and are small compared to the dimensions of the cargo and the saddles.
- Dynamic situations where the deflections of the vessel become large lead to nonlinear behavior. Here a linear approach leads to an overconstrained situation, causing the results to be significantly overestimated.

## 6. Parametric analysis

In order to obtain a better understanding of the considered behavior in relation to different parameters, three different parametric analyses are performed, related to the saddle properties, lashing properties, and cargo properties, respectively. These parameters are varied in a systematic manner while keeping the other properties equal to the ones presented for the base case.

The base case provides the starting values for each of these parameters. For the saddles, significantly more flexible and significantly stiffer versions are tested. These values are meant to represent extremely different cases to the current saddle design and, in this manner, explore the bounds of the design space. The number of saddles is only varied between 2 and 7: with 3 or more saddles, contact nonlinearities are likely to occur, unlike the mostly linear 2-saddle case. Increasing number of saddles (e.g. above 4) could be impractical for this application, due to lack of space and increased installation costs. Therefore, 7 saddles is already considered an extreme value. The approach for lashing stiffness is similar to that for saddle stiffness: significantly (and perhaps impractically) smaller and larger values compared to the base case are used, to identify trends at the bounds of the design matrix. The exact selection of parameters and their effect on the dynamic behavior are discussed in more detail in the following subsections.

### 6.1. Parametric analysis — saddles

In this parametric analysis, the number of saddles is varied in combination with their stiffness. The number of saddles is varied between 2 and 7 while the saddle stiffness is varied between 1 and 1000% of the original stiffness. Note that for simplicity, an equidistant saddle spacing is used over the length of the monopile. This equidistant spacing is defined in a similar manner as shown in Fig. 8, so the saddles cover an equidistant length within the monopile without any saddles at the outer ends.

Fig. 13 shows the results of the analysis for the resulting forces in the sea-fastening system and bending moment in the cargo. The brown grid shown in both figures indicates the region where contact for all saddles is preserved, indicating that linear theory is valid there. Furthermore, for an odd number of saddles both the maximum normal force and maximum bending moment demonstrate local maxima. This is a result of the assumption of an equidistant saddle spacing. For an odd number of saddles one will be located at  $0.5L$  of the monopile, resulting in it carrying the largest load and thereby causing the largest bending moment in the monopile.

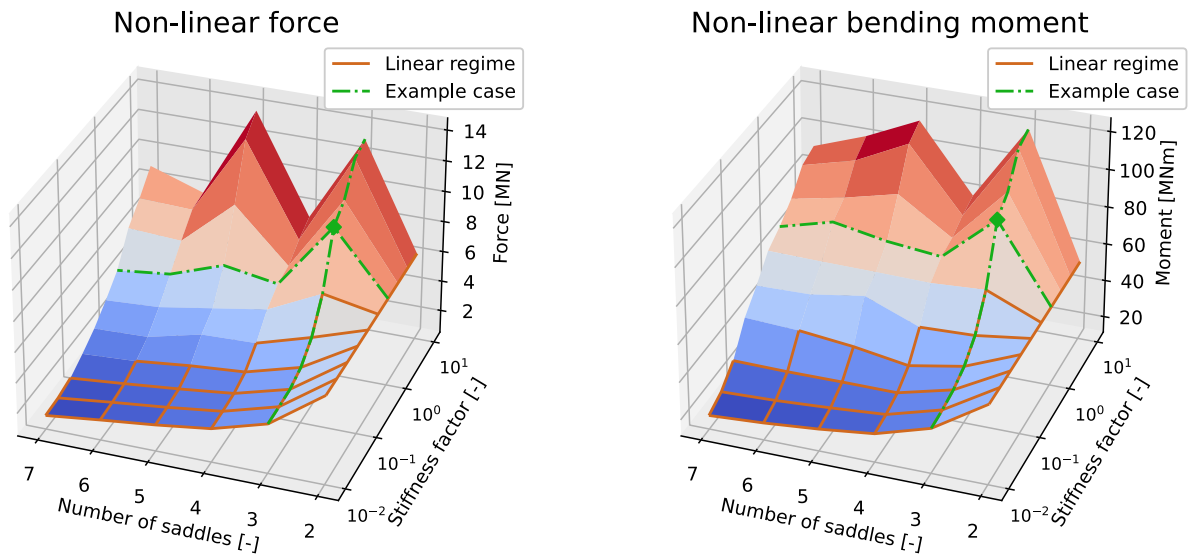


**Fig. 13.** Influence of number of saddles and saddle stiffness on maximum force in sea-fastening system and maximum bending moment in cargo using nonlinear model. The green line represents the case considered in Section 5 and serves as a reference. The brown area indicates domain where contact is preserved and linear theory applies. (For interpretation of the references to color in this figure legend, the reader is referred to the web version of this article.)

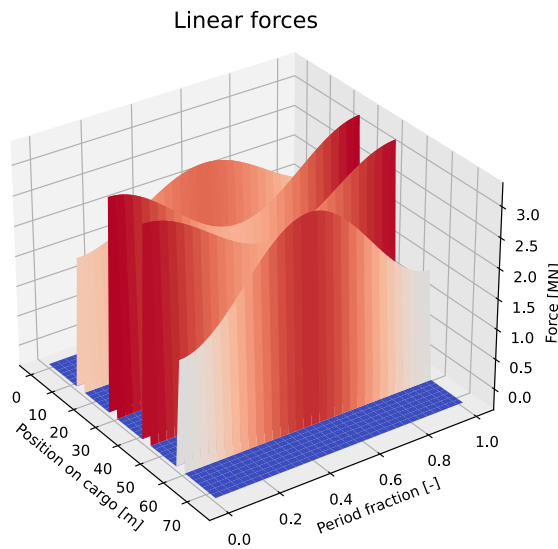


**Fig. 14.** Forces and bending moments acting on monopile for situation with 4 saddles in combination with 10 percent saddle stiffness.

Finally, it is observed that for an increasing number of saddles the transition to nonlinear behavior occurs at a lower stiffness. This is unsurprising, since any additional saddle beyond the first two adds a degree of freedom to an already overdetermined system, generating more opportunities for separation.

The best option to reduce structural loads on the monopile is to have a large number of saddles in combination with a low saddle stiffness. The weight of the monopile can be then distributed over a large number of saddles, leading to lower forces. Furthermore, low saddle stiffness compensates for the bending deflections of the vessel to ensure that its influence on normal force distribution is limited.

To illustrate the above point, Fig. 14 depicts a configuration with 4 saddles and 10% of the original saddle stiffness. When compared to Fig. 12(a), large qualitative and quantitative differences are observed in the dynamic behavior. Contact between the monopile and saddles is preserved when using 4 saddles with lower stiffness, which implies that linear modeling can be applied. Furthermore, the weight of the monopile is more evenly distributed over the 4 saddles. This figure shows that the maximum force in the sea-fastening system is reduced by almost 70%, from 10.5 to 3.3 MN. This decrease in force comes at the cost of an increased deflection of the saddles, which increases approximately by 300%. These and other numerical results are summarized in Table 5.

**Table 5**  
Comparison example case to case with 4 saddles and 10% saddle stiffness.

Parameter		3 Saddles $-1 k_{sad}$	4 Saddles $-0.1 k_{sad}$	Unit
Deflection mon. max.	$u_c$	10.9	5.8	mm
Deflection sad. max.	$u_s$	11.3	35	mm
Detachment max.	$u_d$	11.8	0	mm
Force max.	$F$	10.5	3.3	MN
Bending mom. max.	$M_b$	95.8	38.7	MNm

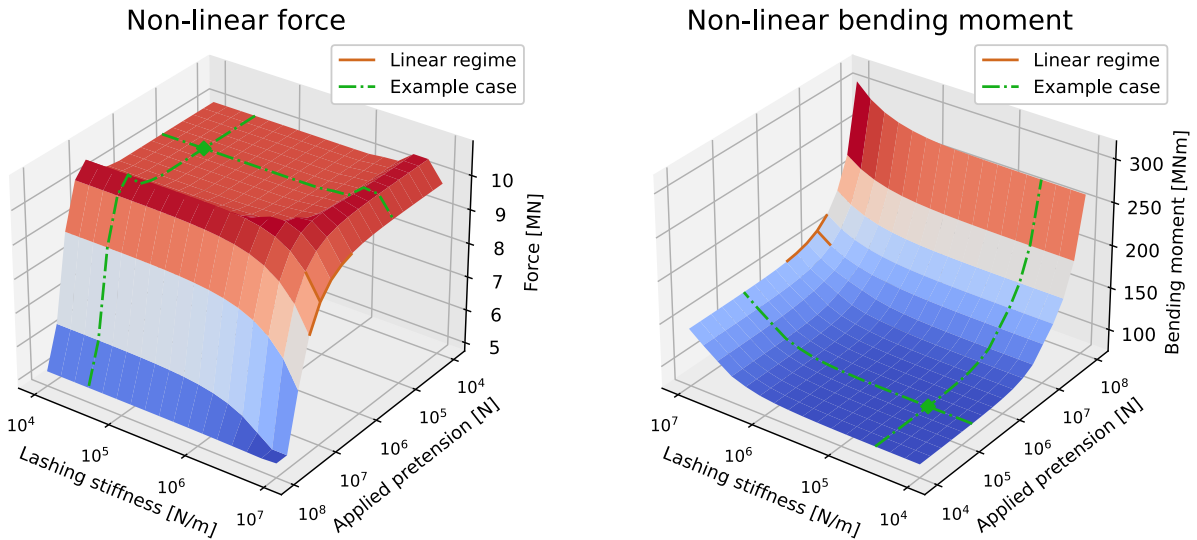


**Fig. 15.** Influence of applied lashing stiffness and pretension on maximum force in sea-fastening system and maximum bending moment in cargo based on nonlinear model. The green lines represent the considered case in Section 5 and serve as a reference. The brown perimeter area indicates again where contact is preserved and linear theory applies. (For interpretation of the references to color in this figure legend, the reader is referred to the web version of this article.)

## 6.2. Parametric analysis — lashing

Another parametric study is performed to investigate the influence of lashing stiffness on the dynamic behavior of the cargo. In this situation the range of lashing stiffness is between  $10^4$  and  $10^7$  N/m, while the range of pre-tension between  $10^4$  and  $10^8$  N.

**Fig. 15** depicts the resulting nonlinear maximum force and the bending moment. Note that the axes origin for the force plot and the bending moment plot are in different locations (back corner and front corner of the xy-plane, respectively), to facilitate visibility. Both subfigures show that, for a large part of the domain, the lashing stiffness and pre-tension do not influence the forces and bending moment in a significant manner. In most cases, the force and bending moment are equal to approximately  $10^4$  to  $10^6$  N and Nm, respectively. This behavior can be explained by the resulting lashing forces being small in comparison to the weight of the monopile and the resulting normal forces at the saddles. Therefore, a negligible influence on the results is observed.

It should be emphasized that it is unlikely that either the lashing stiffness or its pretension will approach the maximum values of  $10^7$  and  $10^8$  in reality. This would indicate a lashing stiffness 300 times larger and a pretension force 500 times larger than what is applied in the base case. Nevertheless, it is useful to explore how the dynamic behavior might be affected when the limits of pretension and stiffness are reached.

## 6.3. Parametric analysis — cargo

Finally, a parametric study is performed with respect to the dimensions of the cargo. The length of the monopile is varied between 75 and 115 m, while the monopile diameter is varied between 8 and 12 m. The monopile considered in the base case is used as a starting point. For this analysis a diameter-to-thickness ratio of 1/110 is chosen.

**Fig. 16** shows the maximum force in the sea-fastening system and the maximum bending stress present in the cargo. In this situation, the bending stress gives more insight into the behavior compared to the bending moment in the monopile. The increase of second moment of area, caused by an increasing diameter and thickness, will result in a lower bending stress for the same bending moment. The figure shows that both force and stress increase with increasing monopile length. This occurs as a result of the weight of the monopile becoming larger, and due to increased unsupported length between the saddles. A higher diameter, on the other hand, results in an increase in force due to the increased weight of the monopile, but a decrease in stress as the increase in second moment of area exceeds the increase in weight. Finally, the increase in weight for a combination of a large length and a large

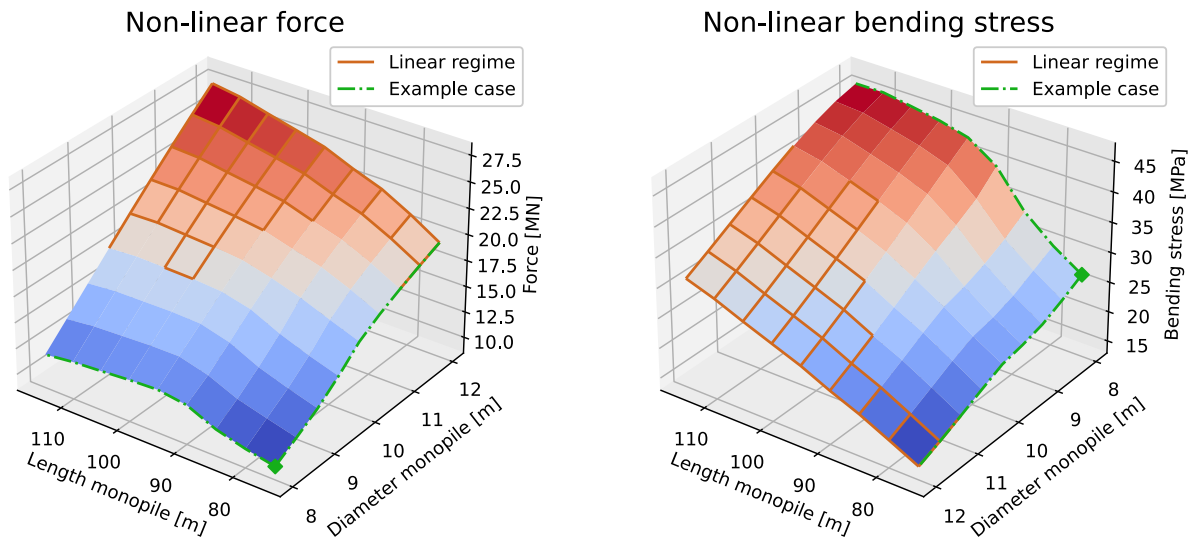


Fig. 16. Influence of length and diameter of cargo on the forces observed in the sea-fastening system and the bending stress in the cargo. The brown area indicates again where linear theory applies and the green lines represent the case considered in Section 5. (For interpretation of the references to color in this figure legend, the reader is referred to the web version of this article.)

diameter leads to the deflection of the monopile becoming large. These large deflections result in contact being preserved for all saddles and linear theory being valid again.

Based on these conclusions two additional cases are identified to further analyze in depth, for the cargo types leading to the highest stress and force response. These include a monopile with a length of 115 m, and a diameter of 8 and 12 m, respectively. For these 2 cases, the parametric saddle analysis is performed again, in order to evaluate to what extent the behavior previously identified still holds for longer and stiffer cargo.

To facilitate the comparison of the results, upper limits for the observed loads were defined. These comprised of a maximum normal force of 7 MN and a maximum bending stress of 20 MPa — approximately 10 percent of the yield stress for mild steel. These upper boundaries for the response should inform us to evaluate various sea-fastening arrangements regarding compliance with the set boundaries.

The subfigures shown in Fig. 17 show the normal force results for a diameter of 8 and 12 m, with a length of 115 m. If compared to Fig. 13 a similar trend is visible, being that the structural response decreases for an increasing number of saddles in combination with lower saddle stiffness. This figure shows that for a diameter of 8 and 12 meters several different sea-fastening arrangements can be selected conforming with the posed upper limits. This indicates that the model can be used to aid in sea-fastening arrangements, defining a number of saddles to comply with a certain maximum force or maximum stress condition. Appendix C shows the results for the bending stress.

## 7. Conclusion

In this investigation, the structural response of a monopile and sea-fastening system is investigated using a finite element model. The monopile and sea-fastening system are subject to displacement-based loads, consisting of hydrodynamic accelerations and wave-induced bending responses of the vessel. Within this analysis the nonlinear properties of the sea-fastening system are taken into account using the harmonic balance as a solution method.

Using the finite element model, different behaviors and sensitivities related to the structural response were investigated for the identified base case. Differences in results for a linear or a nonlinear approach were analyzed in depth. After this thorough analysis of the base case, a large parametric study was performed. In this analysis parameters of various elements present in the cargo-sea-fastening system were varied in order to identify their influence on the structural response. This research presents a new understanding of the structural response when considering stiff cargo. The sensitivity of different parameters on the structural response were quantified and highlighted in the parametric analysis.

The structural response of the monopile and sea-fastening system is defined by the interaction between the bending deflection of the vessel, the axial deflection of the saddles, and the bending deflection of the monopile under its own weight. This interaction influences the weight distribution throughout the system and becomes pronounced in cases when the bending deflection of the vessel becomes greater than the bending deflection of the cargo under its own weight. Then the weight will not be distributed equally throughout the sea-fastening system. The axial deflection of the saddles can compensate for the bending deflection of the vessel, enabling for a better weight distribution in the sea-fastening system.

Nonlinearities occur for dynamic situations with representative saddle stiffness values, and detachment between the monopile and saddles is present. Modeling using a linear approach leads to an overconstrained situation and an overestimation of the structural

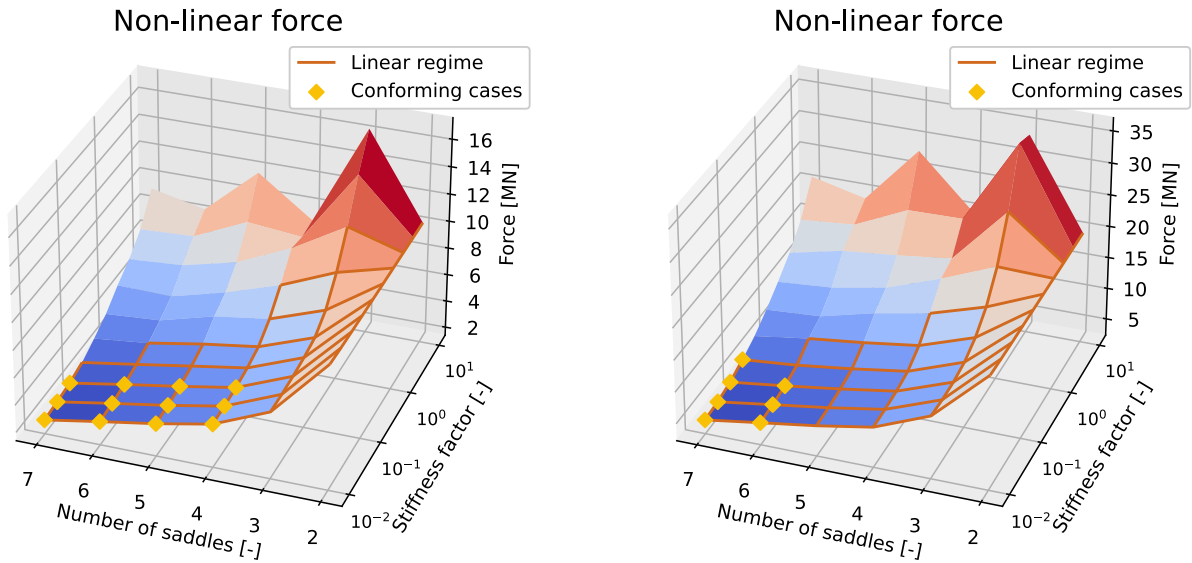


Fig. 17. Influence of number of saddles and saddle stiffness on maximum force in sea-fastening system using nonlinear model. The left and right figure are the results for a monopile with a diameter of 8 and 12 m, respectively.

response. It needs to be emphasized that this behavior is undesirable and indicates inefficient use of the sea-fastening system, since the weight of the cargo is not supported in case of loss of contact.

The parametric analysis showed that a large number of saddles in combination with low stiffness minimizes the loads caused by and transferred to the cargo. In this case the axial deflections of the saddles compensate for the bending deflections of the vessel, ensuring contact between the monopile and saddles. This enables the weight to be distributed more equally over all supports.

No significant influence of lashing properties on structural response is observed — the forces generated by the lashing system stay small in comparison to the weight of the monopile and the resulting normal forces.

The produced model can be used to identify sea-fastening properties for different types of cargo to comply with upper limits posed on the structural response. This research shows that varying the number of saddles in combination with their stiffness systematically helps in design of sea-fastening arrangements.

### CRedit authorship contribution statement

**A.D. Speksnijder:** Writing – original draft, Methodology, Formal analysis. **U. Karacadagli:** Writing – review & editing, Supervision. **H.C. Seyffert:** Writing – review & editing, Supervision. **A. Grammatikopoulos:** Writing – review & editing, Supervision, Conceptualization.

### Declaration of competing interest

The authors declare that they have no known competing financial interests or personal relationships that could have appeared to influence the work reported in this paper.

### Appendix A. Example of bending and inertial forces

Fig. A.1 shows a simple system where the cargo length is chosen to be equal to the vessel length. Furthermore, the sea-fastening system consists of three pinned connections, at  $0L$ ,  $0.5L$  and  $1L$ . The resulting loads for this example are analyzed in detail to give insight in the different loads present in the system.

Fig. A.2 shows the resulting bending moment based on the static and dynamic deflection of the vessel. This dynamic deflection is based on the bending deflection of the vessel subjected to a wave with a length of 171 m, and an amplitude of 1 meter.

Fig. A.3 shows the bending moment resulting from the heave and pitch acceleration combined, for a wave amplitude of 1 meter. This figure shows that the loads resulting from accelerations are significantly smaller compared to the loads caused by forced deflection.



Fig. A.1. Vessel, cargo and sea-fastening system for cargo with equal length to the vessel length. The cargo is connected using a pinned condition at  $0L$ ,  $0.5L$  and  $L$ .

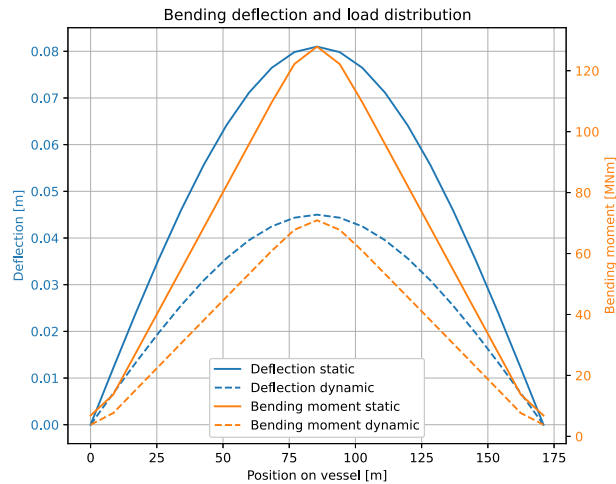


Fig. A.2. Resulting bending moment based on static and dynamic deflection.

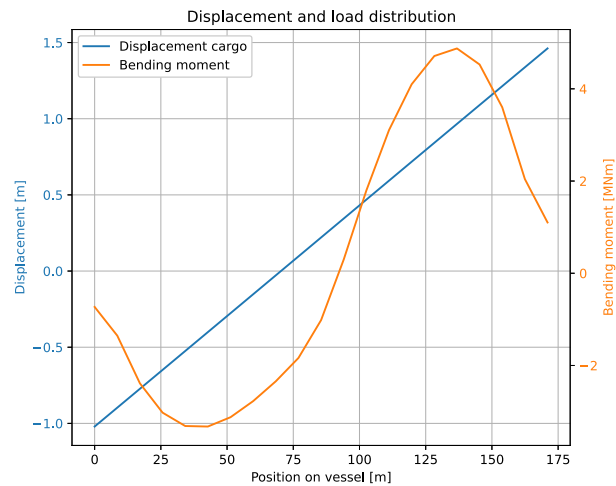


Fig. A.3. Loads based on hydrodynamic heave and pitch acceleration.

### Appendix B. Sensitivity of force distribution under influence of saddle deflection

This appendix highlights an example of the sensitivity of the system in relation to the deflection of the saddles. Figs. B.1 and B.2 show the deflection and load distribution respectively. In this analysis a saddles stiffness of half the actual value is assumed; Table B.1 shows the corresponding results. This table shows that the deflection of the monopile decreases while the deflection of the saddles increases. These differences in deflections influence the load distribution significantly.

This analysis shows that the structural response of the cargo is defined by the interaction of the bending deflection of the vessel, the axial deflection of the saddles, and the bending deflection of the cargo. Furthermore, this analysis also highlights the necessity to model the axial deflection of the saddles correctly.

**Table B.1**  
Results for static load case using half saddles stiffness.

Parameter		$1 \cdot k_{sad}$	$0.5 \cdot k_{sad}$	Unit
Deflection mon. max.	$u_c$	5.9	4.8	mm
Deflection sad. max.	$u_d$	5.7	9.5	mm
Force max.	$F$	6.3	4.9	MN
Bending mom. max.	$M_b$	49.3	37.2	MNm

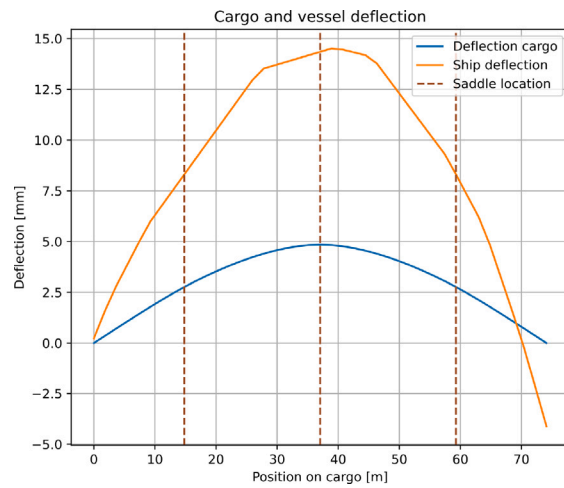


**Fig. B.1.** Deflection of ship, saddles and monopile for saddles with half stiffness.

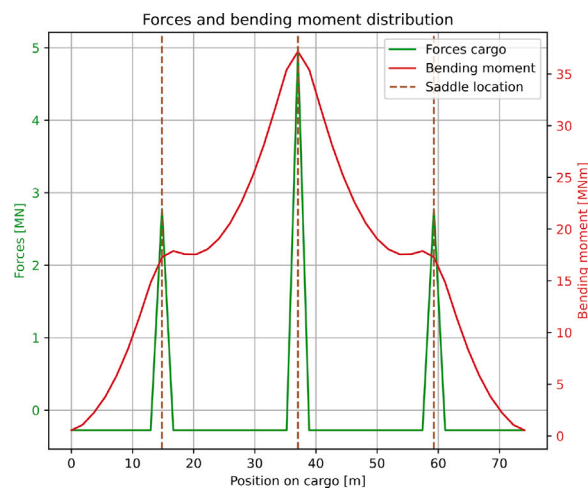


**Fig. B.2.** Forces and bending moments acting on monopile for saddles with half stiffness.

## Appendix C. Additional results cargo parametric analysis

This appendix presents some additional results related to the cargo parametric analysis. Figs. C.1 and C.2 show the magnitude of the bending stress of the cargo for a diameter of 8 and 12 meters respectively. Similar behavior as in Fig. 17 is observed. Based on these figures the conclusion can be drawn that for a monopile of 8 meters in diameter the arrangements are limited by the bending stress criterion, while for a diameter of 12 meters arrangements are limited by the force criterion.

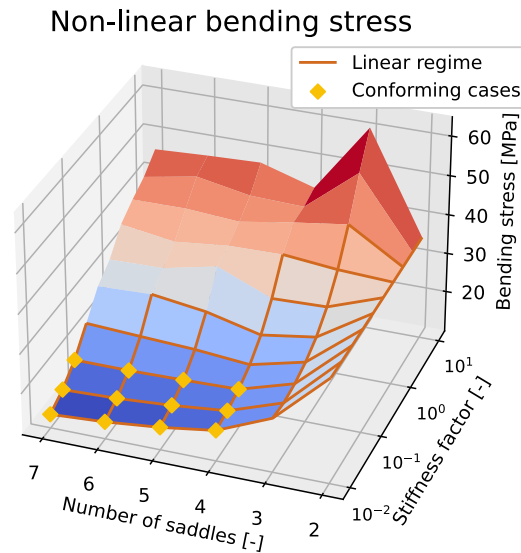


Fig. C.1. Bending stress response for monopile of 8 meters in diameter.

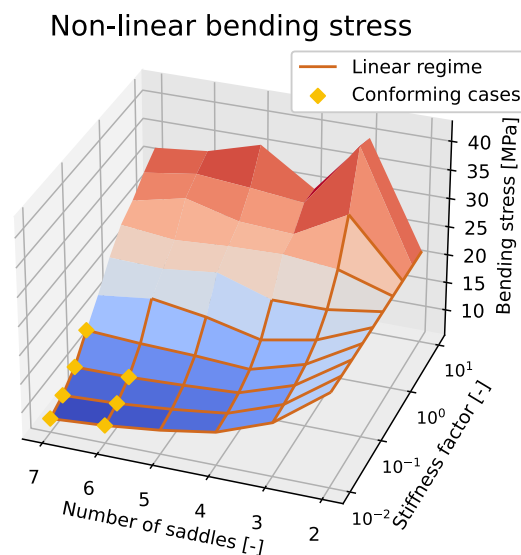


Fig. C.2. Bending stress response for monopile of 12 meters in diameter.

### Data availability

Data will be made available on request.

### References

- [1] H-blix, Offshore wind vessel availability until 2030: Baltic Sea and Polish perspective-Offshore wind vessel availability until 2030: Baltic Sea and Polish perspective Final Report, in: Technical Report, 2022, URL [www.h-blix.com.pl](http://www.h-blix.com.pl).

- [2] A. Fernandez-Guillamon, K. Das, N.A. Cutululis, A. Molina-Garcia, Offshore wind power integration into future power systems: Overview and trends, *J. Mar. Sci. Eng.* 7 (11) (2019) 399.
- [3] M. Shadlou, S. Bhattacharya, Dynamic stiffness of monopiles supporting offshore wind turbine generators, *Soil Dyn. Earthq. Eng.* 88 (2016) 15–32, <http://dx.doi.org/10.1016/j.soildyn.2016.04.002>, URL <https://www.sciencedirect.com/science/article/pii/S0267726116300069>.
- [4] K.H. Chua, Y. Zhang, D. Konovessis, Cargo Liquefaction and Influence on Ship Stability, in: *International Conference on Offshore Mechanics and Arctic Engineering*, 58776, American Society of Mechanical Engineers, 2019, V002T08A054.
- [5] W. Chen, A. Roberts, A. Katterfeld, C. Wheeler, Modelling the stability of iron ore bulk cargoes during marine transport, *Powder Technol.* 326 (2018) 255–264, <http://dx.doi.org/10.1016/j.powtec.2017.12.006>, URL <https://www.sciencedirect.com/science/article/pii/S0032591017309610>.
- [6] T.P. Rocha, R. Dotta, D.P. Vieira, P.C.d. Mello, E.B. Malta, K. Nishimoto, Experimental investigation on the influence of liquid cargo in floating vessels motions, in: *OTC Brasil, OnePetro*, 2015.
- [7] J.J. Park, H. Kawabe, M.-S. Kim, B.W. Kim, M.K. Ha, Numerical sloshing assessment including tank sloshing and ship motion coupling effect, in: *Proceedings of the International Offshore and Polar Engineering Conference*, vol. 3, 2010, pp. 237–243.
- [8] S. Mitra, C.Z. Wang, J.N. Reddy, B.C. Khoo, A 3D fully coupled analysis of nonlinear sloshing and ship motion, *Ocean Eng.* 39 (2012) 1–13, <http://dx.doi.org/10.1016/j.oceaneng.2011.09.015>, URL <https://www.sciencedirect.com/science/article/pii/S0029801811002095>.
- [9] H.-W. Lee, M.-I. Roh, Review of the multibody dynamics in the applications of ships and offshore structures, *Ocean Eng.* 167 (2018) 65–76, <http://dx.doi.org/10.1016/j.oceaneng.2018.08.022>, URL <https://www.sciencedirect.com/science/article/pii/S0029801818315178>.
- [10] N. Ku, M.-I. Roh, Dynamic response simulation of an offshore wind turbine suspended by a floating crane, *Ships Offshore Struct.* 10 (6) (2015) 621–634.
- [11] H. Hatecke, S. Krüger, J. Christiansen, H. Vorhölter, A fast sea-keeping simulation method for heavy-lift operations based on multi-body system dynamics, in: *International Conference on Offshore Mechanics and Arctic Engineering*, 45370, American Society of Mechanical Engineers, 2014, V01AT01A032.
- [12] O. Solovey, A. Ben, S. Dudchenko, P. Nosov, Development of control model for loading operations on Heavy Lift vessels based on inverse algorithm, 5, (2–107) (ISSN: 1729-3774) 2020, pp. 48–56.
- [13] M.A. Hannan, W. Bai, Nonlinear hydrodynamic responses of submerged moving payload in vicinity of a crane barge in waves, *Mar. Struct.* 41 (2015) 154–179, <http://dx.doi.org/10.1016/j.marstruc.2015.01.002>, URL <https://www.sciencedirect.com/science/article/pii/S0951833915000118>.
- [14] D. Mikail, M. Teunis, A. Grammatikopoulos, Ship-cargo Interaction for Vessels Carrying Large Wind Turbine Monopiles, in: *9th International Conference on Hydroelasticity in Marine Technology*, 2022, pp. 41–50.
- [15] Y. Colaïtis, A. Batailly, The harmonic balance method with arc-length continuation in blade-tip/casing contact problems, *J. Sound Vib.* 502 (2021) 116070.
- [16] T. Vadcard, A. Batailly, F. Thouverez, On Harmonic Balance Method-based Lagrangian contact formulations for vibro-impact problems, *J. Sound Vib.* 531 (2022) 116950, <http://dx.doi.org/10.1016/j.jsv.2022.116950>, URL <https://www.sciencedirect.com/science/article/pii/S0022460X22001791>.
- [17] M. Attar, A. Karrech, K. Regenauer-Lieb, Non-linear modal analysis of structural components subjected to unilateral constraints, *J. Sound Vib.* 389 (2017) 380–410.
- [18] E.H. Moussi, S. Bellizzi, B. Cochelin, I. Nistor, Nonlinear normal modes of a two degrees-of-freedom piecewise linear system, *Mech. Syst. Signal Process.* 64–65 (2015) 266–281, <http://dx.doi.org/10.1016/j.ymsp.2015.03.017>, URL <https://www.sciencedirect.com/science/article/pii/S0888327015001430>.
- [19] M. Attar, A. Karrech, K. Regenauer-Lieb, Non-linear analysis of beam-like structures on unilateral foundations: A lattice spring model, *Int. J. Solids Struct.* 88 (2016) 192–214.
- [20] G.N. Wells, The Finite Element Method: An Introduction, in: *Technical Report*, 2009, pp. 113–125.
- [21] M. Krack, J. Gross, *Harmonic Balance for Nonlinear Vibration Problems*, vol. 1, Springer, 2019.
- [22] M. Peeters, R. Vigué, G. Sérandour, G. Kerschen, J.C. Golinval, Nonlinear normal modes, Part II: Toward a practical computation using numerical continuation techniques, *Mech. Syst. Signal Process.* 23 (1) (2009) 195–216, <http://dx.doi.org/10.1016/J.YMSSP.2008.04.003>.
- [23] F. Schreyer, R.I. Leine, A mixed shooting-harmonic balance method for unilaterally constrained mechanical systems, *Arch. Mech. Eng.* 63 (2) (2016) 297–314.
- [24] B. Cochelin, Numerical computation of nonlinear normal modes using HBM and ANM, *Modal Anal. Nonlinear Mech. Syst.* (2014) 251–292.